Advanced Modelling of Polyoxometalate Counter-Cations: Bridging Explicit Counter-Cation Inclusion and Solvent Effects for Electronic Applications

*Jake Jacobs,[1] María José Aliaga-Gosalvez[1] Vihar P. Georgiev[*2] and Laia Vilà-Nadal[*1]*

[1]*School of Chemistry, University of Glasgow, Glasgow, UK*

[2]*Device Modelling Group, James Watt School of Engineering, University of Glasgow, Glasgow, UK*

KEYWORDS: Polyoxometalates (POMs), Computational Chemistry, Density Functional Theory (DFT), Counter-Cation Interaction, Molecular Electronics, Frontier Orbital Energies.

Abstract

This study explores the explicit modelling of polyoxometalate (POM) counter-cations in both solid states and solutions, focusing on their potential for integration into molecular electronics, specifically as components of single-molecule electronic devices. Employing Density Functional Theory (DFT) and the Conductor-like Screening Model (COSMO), our research addresses the challenge of accurately representing the environmental effects on POMs, particularly the influence of counter-cations and solvent molecules. A critical finding of this work is the demonstration that traditional models, like COSMO, often fail to capture the physical distancing effects of solvents, leading to an overestimation of the proximity of counter-cations to POM anions and resulting in over-stabilized frontier orbital energies. By implementing geometry constraints on lithium cations, we achieve a more realistic depiction of POM-cation interactions in solution, enhancing model accuracy. Additionally, our results

suggest that explicit counter-cation inclusion is essential for accurate simulations pertinent to POM applications in electronic devices, though it can be computationally intensive in solution environments. This study not only advances the theoretical understanding of POMs but also underscores the need for improved computational strategies to simulate real-world conditions effectively, thereby guiding the development of POM-based electronic components.

Introduction

POMs properties and applications

Polyoxometalates (POMs) are a diverse class of inorganic compounds, molecular metal oxides composed of early transition metals like molybdenum (Mo) and tungsten (W) in their highest oxidation states, combined with oxide anions[1]. POMs form a variety of large, highly-charged anionic clusters, balanced with a range of counter-cations[2]. There are several polyanion architectures, including Lindqvist ($[M_6O_{19}]^{2-}$), Keggin ($[XM_{12}O_{40}]^{n-}$), and Wells-Dawson ($[X_2M_{18}O_{62}]^{n-}$) frameworks, each distinguished by the unique count, configuration, and connectivity of their constituent metal oxide polyhedra[3], where M is typically Mo and W and X, is a heteroatom such as silicon (Si), phosphorus (P), or arsenic (As): in isopolyoxometalates the heteroatoms are absent[4,5].

The extensive variability of POMs motivates a rich field of research [6]: in fact, POMs are the target of investigations across a range of fields including catalysis [7–9], medicine[10–12], energy storage [13–15], and notably, molecular electronics[16–19]. This study focuses on the integration of POMs into molecular electronics, particularly as components in flash memory devices. This aptness for this application is down to POMs high thermal stability[20,21], nanoscale dimensions, and unique redox characteristics[22–24], aligning with the continuous drive towards device miniaturization and energy efficiency. As such, POMs are of special interest in the context of single-molecule electronics[25,26]. Therefore, this research delves into the explicit modelling of POM counter-cations as single molecules (ionic compounds) both in solid state and in solution, building upon foundational studies that have illuminated the potential of

POMs in memory device applications [21,22,27–31] and in some cases, demonstrated that the electron transport properties are significantly influenced by the identity of the counterion [32].

POMs and DFT

Computational modelling, particularly Density Functional Theory (DFT), is a widely used tool in the study and characterization of POMs [33–36]. Theoretical analysis of POMs through DFT, provides insights into their electronic structures and properties, guiding experimental efforts and theoretical understanding[37–39]. However, one of the challenges of realistic theoretical modelling of POMs lies in accounting for influence of the immediate environment, this includes the effects of solvent and counter-cations [27,33,40–43]. Both the solvent and counter-cations serve to stabilise the POMs anionic charge and, as such, these factors influence on the electronic properties of POMs[42].

The influence of solvent and counter-cation environment can be determined through investigating frontier orbital energies, since they are key indicators of a molecule's electronic structure [44]. As such, these parameters are instrumental in determining POMs' reactivity, stability, catalytic effectiveness, and their electronic and optical characteristics. The energy levels of HOMO and LUMO are particularly significant in the context of molecular electronics because charge transport capabilities depend on the accessibility of energy states near the HOMO and LUMO levels [42,45]. DFT is particularly useful in these investigations since it provides a higher level of detail than can be determined by empirical methods alone. This current study's approach uses DFT calculations to examine the effect POM environment though investigation of frontier orbital energy and their implications for memory device integration. We hypothesise that the explicit modelling of counter-cations in conjunction with POMs can yield novel insights into the material's suitability for electronic applications, particularly memory devices[39,42]. Notably, this includes modelling POMs in vacuum with explicit counter-cations in order to best replicate the state in which POMs will operate as part of components in memory devices, particularly in the context of single-molecule electronics.

POMs, Continuum Solvent Models (COSMO) and Counter-cation interactions

One theoretical method employed to account for solvent effects, the Conductor-like Screening Model (COSMO)[46–48] has proven to be an effective and pragmatic option [41,48,49]. COSMO, a continuum solvent model, offers a less computationally intensive alternative for incorporating solvent influences compared with modelling explicit solvent [40,48]. It treats the solvent as a structureless continuum, simplifying the computational demands while providing a reasonable approximation of solvent effects [49]. COSMO has been employed in this study to simulate the solvent environment's impact on the POMs' properties. Part of the rationale for using COSMO comes from a study conducted by Miró et al.[41], who demonstrate comparability between explicit solvent models and COSMO in stabilizing the electronic structures of POMs, particularly in terms of Keggin anions ($[XM_{12}O_{40}]^{n-}$, where X= P, Si, As, etc. and M= Mo^{6+}, W^{6+}). These investigations reveal that while detailed, explicit models provide nuanced insights, COSMO remains a robust alternative, adequately mirroring the solvation effects, especially when focusing on the electronic stabilization crucial for theoretical predictions. Miró et al. also consider counter-cations in their theoretical models, however, they model counter-cations as point charges rather than explicitly including the counter-cations in the model as with this current study. As such, we develop previous models by employing a higher level of precision and a greater range of POM anions and of explicit counter-cations; Figure 1 shows the range of POMs used in this study. We also employ exchange-correlation functional PBE0[50–52] along with GGA BP86[53,54] in an effort to examine the additional effect of functional on the investigation of the effects of POM environments.

Another significant advancement in this study is the examination of the limitations inherent to the COSMO continuum solvent method in combination with counter-cations, namely its failure to simulate the physical effects of solvent molecules on the proximity of counter-cations to POM anions. This limitation can lead to an overstabilization of frontier orbitals, a consequence of unrealistic counterion-POM proximities, shorter distances than would occur under actual solvent conditions. By adopting a more rigorous approach that includes constraining the geometry of Li+ cations, this research endeavours to overcome these shortcomings, aiming for a more authentic representation of POM-cation interactions in solution. This methodological refinement is not merely a technical adjustment but a crucial step

towards ensuring that our theoretical models mirror real-world conditions as closely as possible, thus enhancing the reliability of our predictions and findings.

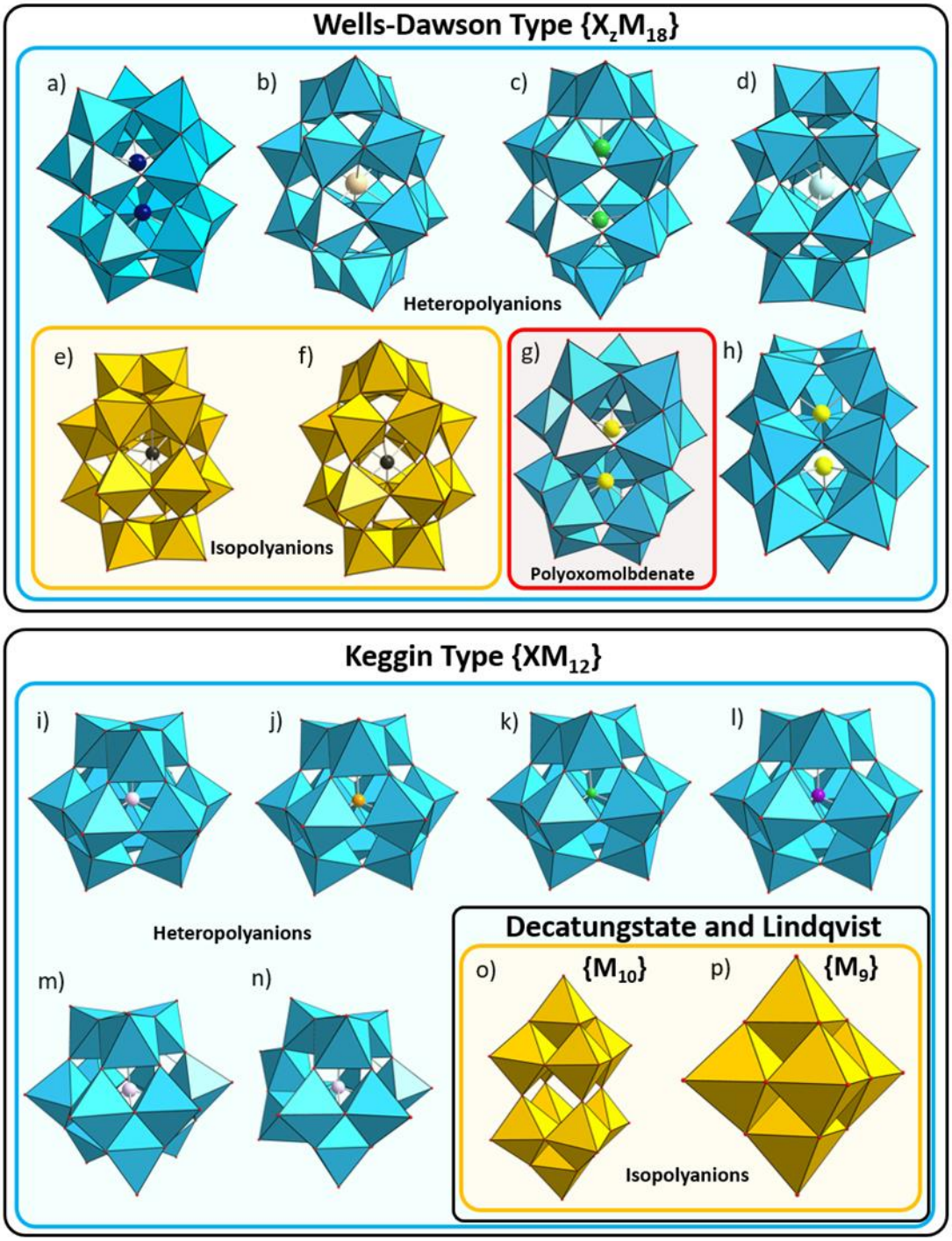

Figure 1. Polyhedral and ball and ball-and-stick model (B&S) representation of the range of POM anions considered in this study; geometry optimised with BP86 functional in vacuum. Colour code: O: red; Heteropoly anions: blue polyhedra; a) $[W_{18}O_{54}(SeO_3)_2]^{4-}$ Se: dark blue B&S; b) β*-$[W_{18}O_{56}(IO_6)]^{9-}$, I: white c) α-$[W_{18}O_{54}(PO_4)_2]^{6-}$ P: green d) γ*-$[W_{18}O_{56}(TeO_6)]^{10-}$ Te: pale blue; Isopolyanions: yellow polyhedra e) α-$[W_{18}O_{56}(WO_6)]^{10-}$ $W_{central}$: black f) γ*-$[W_{18}O_{56}(WO_6)]^{10-}$; g) $[Mo_{18}O_{54}(SO_3)_2]^{4-}$ h) $[W_{18}O_{54}(SO_3)_2]^{4-}$ S: yellow; i) α-$[SiW_{12}O_{40}]^{4-}$ Si: white; j) α-$[GeW_{12}O_{40}]^{4-}$ Ge:

yellow; k) α-$[PW_{12}O_{40}]^{3-}$ P: green; l) α-$[AsW_{12}O_{40}]^{3-}$ As: purple; m) β –$[SiW_{12}O_{40}]^{4-}$ Si: white; n) γ – $[SiW_{12}O_{40}]^{4-}$ Si: white; o) $[W_{10}O_{32}]^{4-}$; p) $[W_6O_{19}]^{2-}$.

Implications, relevance and summary

This study represents a development on previous work[27] in that it includes explicit counter-cations along with solvent in theoretical calculations which evidence their effects on frontier orbital energies. Our research is driven by the critical relevance of POMs' frontier orbital energies, particularly the absolute energy levels rather than relative differences, due to their significant implications in electrochemistry and molecular electronics applications. Accordingly, with the view to realistically modelling POMs for use in memory devices, this study also models POMs with explicit counter-cations in vacuum in order to replicate the environmental conditions of POMs used for this purpose. We question whether continuum solvent methods can serve as a proxy for a counter-cation environment. Building upon the foundational insights offered by previous studies, including the examination of $[W_{18}O_{54}(SeO_3)_2]^{4-}$ polyoxometalates for memory device applications, this research extends the inquiry to a broader array of POMs and to the hybrid exchange-correlation functional, PBE0 alongside the GGA functional, BP86, in order to strengthen the generalisability of our findings.

Computational Details

Different non-classic Wells-Dawson, Deca-tungstate and Keggin geometries have been fully optimized at the DFT level using the ADF package of the Amsterdam Modelling Suite (AMS 2021.1).[55,56] The exchange-and-correlation functional functionals used in the calculations in this study are BP86, PBE0, and, B3LYP. BP86 is a generalized gradient approximation (GGA) density functional[57,58], PBE0 an B3LYP are the hybrid which combine a standard GGA with a Hartree-Fock exchange part[59–61]. Each functional was used in combination with TZP basis set[62], a large frozen core for BP86, and no frozen core for PBE0 and B3LYP, since previous studies have demonstrated their suitability for these types of calculations.[33,40,63,64] Relativistic effects were accounted for using the ZORA formalism.[65–69] Solvent effects were considered using the Conductor-like Screening Model (COSMO)[70] - included in the ADF package[48] with conventional van der Waals values for solvation radii established for ADF.[71,72]

Results and Discussion

Frontier orbitals energies, geometries, HOMO-LUMO gaps and molecular electrostatic potential (MEP) mappings have been plotted for the following POMs (shown in Figure 1): $[W_{18}O_{54}(SeO_3)_2]^{4-}$, β*-$[W_{18}O_{56}(IO_6)]^{9-}$, α-$[W_{18}O_{54}(PO_4)_2]^{6-}$, γ*-$[W_{18}O_{56}(TeO_6)]^{10-}$, α-$[W_{18}O_{56}(WO_6)]^{10-}$, γ*-$[W_{18}O_{56}(WO_6)]^{10-}$, $[Mo_{18}O_{54}(SO_3)_2]^{4-}$, $[W_{18}O_{54}(SO_3)_2]^{4-}$, α-$[SiW_{12}O_{40}]^{4-}$, α-$[GeW_{12}O_{40}]^{4-}$, α-$[PW_{12}O_{40}]^{3-}$, α-$[AsW_{12}O_{40}]^{3-}$, β -$[SiW_{12}O_{40}]^{4-}$, γ -$[SiW_{12}O_{40}]^{4-}$, $[W_{10}O_{32}]^{4-}$, $[W_6O_{19}]^{2-}$. The metal selected for the majority of the POMs used in this study is tungsten. This is because tungsten-polyanions (tungstates) are typically more structurally resilient and are stable at higher temperatures than the other common alternatives such as molybdates.[21,73] This is significant for this project because the candidate POMs are required to be stable at the high temperatures used for device fabrication.

Effect of the functional

We investigated the impact of different functionals (BP86, B3LYP, PBE0) on the frontier orbital energies and HOMO-LUMO gaps of all candidate POMs. As shown in Figures 2 and 3, the HOMO-LUMO gaps calculated using BP86 were consistently smaller than those obtained with the hybrid functionals (B3LYP and PBE0). Moreover, the HOMO-LUMO gap range for BP86 fell within the range of B3LYP, which, in turn, was within the range of PBE0. These findings align well with previous studies,[74] including reported López et al.'s review.[40] This same review evidenced that BP86, particularly in combination with TZP basis set, is adequate for determining frontier orbital energies. However, the large discrepancy between the frontier orbital energies calculated with GGA and with hybrid functionals and also the HOMO-LUMO gaps, compelled us to continue with both GGA with hybrid functionals - in spite of the fact that hybrid functionals are computationally more expensive [ref]. Thus, our findings are more generalisable: indeed, we found the same patterns present regardless of functional despite continued discrepancies between frontier orbital energies and HOMO-LUMO gaps.

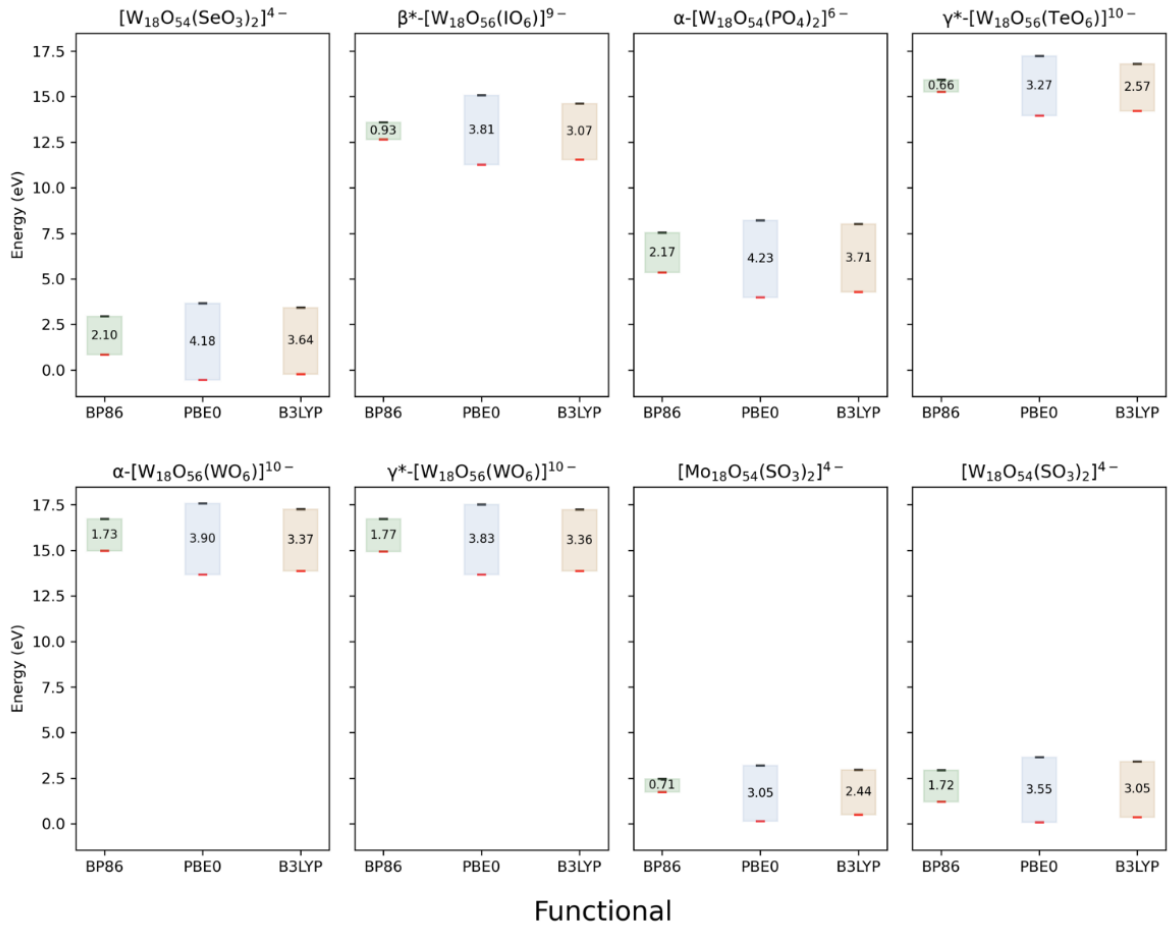

Figure 2. Comparison of different functionals BP86, B3LYP and PBE0 for calculation of the HOMO-LUMO energies in eV of POM anions with Wells-Dawson framework $\{X_zW_{18}\}$. The energy of the LUMO is indicated by black horizontal lines, the energy of the HOMO is indicated by red horizontal line and, the HOMO-LUMO gap (eV) is labelled in between.

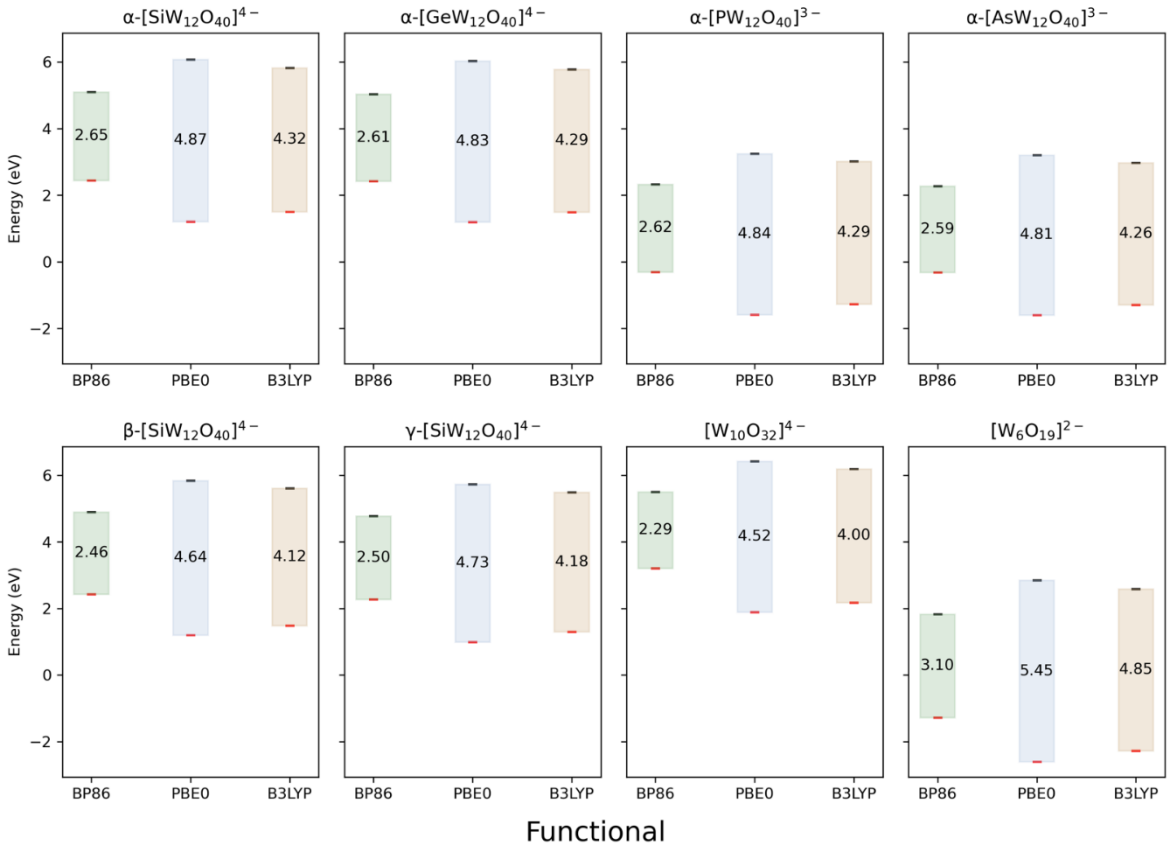

Figure 3. Comparison of BP86, B3LYP and PBE0 functionals for calculation of the HOMO-LUMO energies in eV of POM anions with Keggin $\{XW_{12}\}$, Deca-tungstate $\{W_{10}\}$ and Lindqvist $\{W_9\}$ frameworks. The energy of the LUMO is indicated by black horizontal lines, the energy of the HOMO is indicated by red horizontal line and, the HOMO-LUMO gap (eV) is labelled in between.

Solvent effects (Continuum solvent model)

To assess the impact of solvent on POM properties, we employed the COSMO continuum solvent model with water and acetonitrile respectively as solvents across the same range of POM anions. The results, revealed that solvation stabilised the energies of the frontier orbitals, as expected. The magnitude of the HOMO-LUMO gap remained largely unaffected by solvation in line with previous work[41], indicating that this parameter remains a reliable descriptor of stability across both conditions. We observed minimal differences between the two solvents, water and acetonitrile, further suggesting that solvent choice has limited impact on the HOMO-LUMO gap magnitude. However, further investigation using a broader range of solvents should be conducted in future work, especially given that water and

acetonitrile have comparable polarity. An extremely strong correlation is observed between solvation stabilisation and charge of the POM anion, shown in Figure 4, which indicates that POM-anion charge is the main factor which determines the magnitude of the stabilisation which results from solvation.

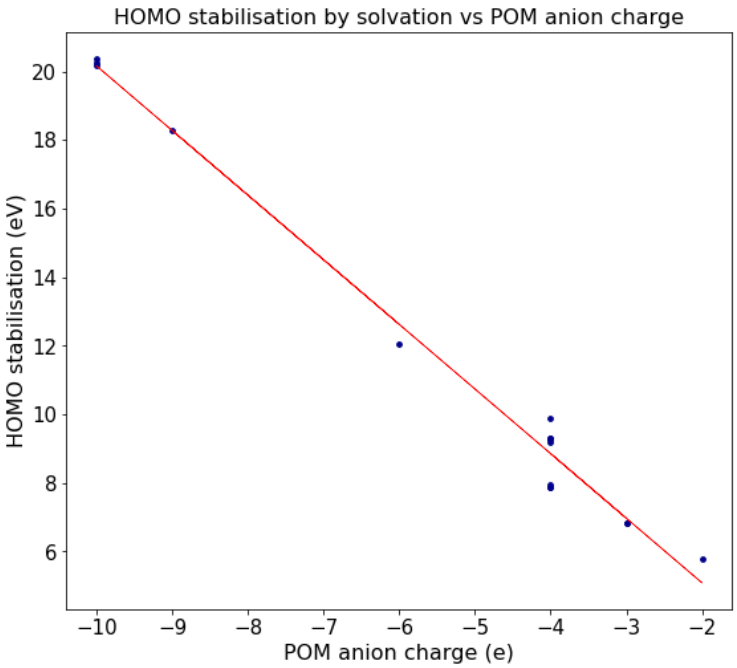

Figure 4. HOMO stabilisation by solvation vs POM anion charge. The HOMO stabilisation was calculated by finding the difference between the absolute value of the HOMO energy for the POM in a vacuum and the absolute value of the HOMO energy for the solvated POM (taken as the mean average between calculations conducted in water and acetonitrile. The values were calculated with DFT calculations which used the BP86 functional and COSMO to model the solvation.

Effect of explicit counter-cations

To examine the effect of including explicit counter-cations in our theoretical models we focused on a narrower range of POMs, $[W_{18}O_{54}(SeO_3)_2]^{4-}$, α-$[W_{18}O_{54}(PO_4)_2]^{6-}$, α-$[SiW_{12}O_{40}]^{4-}$, α-$[PW_{12}O_{40}]^{3-}$, and $[W_{10}O_{32}]^{4-}$. We modelled POMs with explicit lithium (Li^+), tetramethyl ammonium (TMA^+), tetrabutyl ammonium (TBA^+) counter-cations both in vacuum and solvent environments to investigate their influence on the stability, frontier orbital energies, HOMO-LUMO gaps and charge distribution of POMs. We performed these calculations with both BP86 and PBE0 exchange-correlation functionals to examine the effect of functional of these calculated values. This was achieved by performing geometry

optimisation calculations, or in the case of more computationally expensive calculations (PBE0 with Well-Dawson POMs and explicit counter-cations), single-point calculations using a previously optimised geometry.

In line with previous studies [2,42], our calculations evidence the stabilising effect of a counter-cation environment on POM frontier orbital energies. Figure 5 shows the frontier orbital energies of Keggin α-$[PW_{12}O_{40}]^{3-}$ POM salts in vacuum. The same pattern is observed for each of the POMs modelled in vacuum for this study: counter-cations stabilised the frontier orbitals by between 6 and 9eV; the HOMO-LUMO gap remains fairly constant; and Li^+ has the greatest stabilising effect compared with the alkylammonium cations. The large discrepancy between the BP86 and PBE0 functionals also remained. The fairly constant HOMO-LUMO gap, similar to the results observed in water and acetonitrile solvents, demonstrates that both the HOMO and LUMO are stabilised to the same degree by their immediate environment. In contrast, the immediate environment has a large effect on the absolute energies of the frontier orbitals. Li^+ counter-cations induced the largest stabilizations and were accompanied by the largest HOMO-LUMO gaps. This effect can be attributed to the smaller size of Li^+ ions, leading to a higher charge density and closer POM-counter-cation distances, significantly impacting the frontier orbital energies. Interestingly, the effects of TMA^+ and TBA^+ counter-cations were nearly identical, suggesting their comparable influence on the POM properties.

This current study demonstrates that POM frontier orbital energies are counter-cation dependent under vacuum. Moreover, explicit counter-cations with vacuum are the conditions which best replicate a solid-state environment, particularly suitable in the context of single-molecule electronics. Our calculations demonstrate that the identity of the counter-cation affects the frontier orbital energies: there is differential stabilisation by the Li^+ and alkylammonium cations. As such, models which attempt to replicate these conditions should employ explicit counter-cations in order to ensure the accuracy of their calculations.

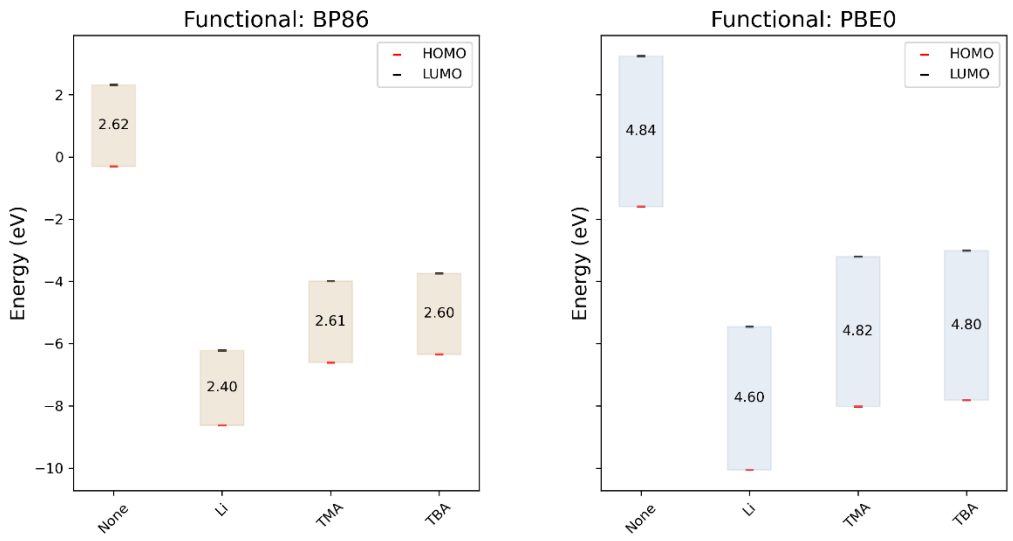

Figure 5. Comparison of explicit counter-cation incorporation for calculation of the HOMO-LUMO energies of α-$[PW_{12}O_{40}]^{3-}$ Keggin POM salts in vacuum. The energy of the LUMO is indicated by black horizontal lines, the energy of the HOMO is indicated by red horizontal line and, the HOMO-LUMO gap (eV) is labelled in between. The left facet shows results using BP86 functional, the right facet shows results using PBE0 functional.

Initially, this same dependence on counter-cation identity was observed with the addition of solvent into the model, however, in this case, this was attributable to a neglect of POM-cation distance. As previously mentioned, one issue with using the COSMO method models which include explicit counter-cations is that it doesn't consider how solvent molecules affect the distance between cations and POM anions.[75] This arises because it models the solvent as a homogenous medium, rather than explicit solvent molecules which form solvent shells around charged species. In reality, solvent shells results in a minimum distance between POM and cation. Failing to take this minimum distance into account means that counter-cations exert an exaggerated influence on POMs' electron distribution and stability, diverging from behaviours noted in actual solvent conditions. Kaledin et al. further explores this discrepancy, suggesting that the COSMO model inadequately represents the bulk effects of aqueous solutions on POMs, particularly concerning the spatial arrangements of counter-cations.[76]

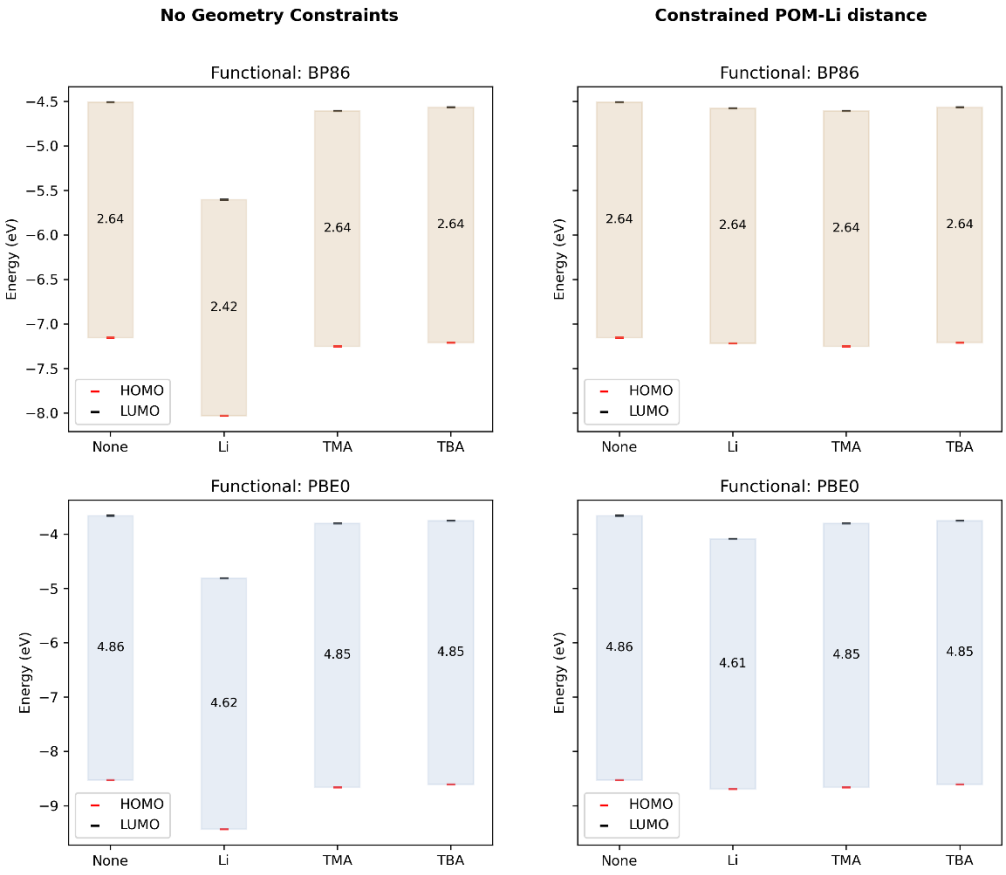

Figure 6. Comparison of explicit counter-cation incorporation for calculation of the HOMO-LUMO energies of α-$[PW_{12}O_{40}]^{3-}$ Keggin POM salts in water. The energy of the LUMO is indicated by black horizontal lines, the energy of the HOMO is indicated by red horizontal line and, the HOMO-LUMO gap (eV) is labelled in between. The left column shows results were obtained without constraining the POM-Li^+ distance, the right column shows results where the POM-Li^+ distance was constrained (cation-heteroatom distance = 9.1 Å).

Distances between the alkylammonium cations and central heteroatom calculated in this current study matched previous work, which crucially was empirically grounded by ^{31}P-NMR [77]. Thus, it was not necessary constrain the geometries for POM-TMA and POM-TBA distances during geometry optimisation calculations. In contrast, the optimised geometries calculated where Li^+ was the counter-cation resulted in unrealistically short POM-cation distances. We attribute this weakness in the model to the fact that Li^+ a far higher charge density that the alkylammonium cations, therefore, it is solvated

to a greater extent. As such, constraining the geometry becomes important. Previous work by Kaledin *et al*.[76] show that with Li, and explicit water molecules the average distance between Li and the central heteroatom of α-$[PW_{12}O_{40}]^{3-}$ POM was 9.1Å. Accordingly, we repeated our geometry optimisation calculations using the ADF to constrain the geometry of the Li^+ cations to 9.1Å from the central heteroatom. In the Wells-Dawson and Decatungstate POM structures, no central heteroatom is present. In these case, a dummy atom was inserted at the centre of the POM anion and this was used to constrain the geometry. As shown in Figure 6 and 7, the increased distance led to less stabilisation of the frontier orbital energies than when the Li^+ was allowed to approach the POM anion too closely.

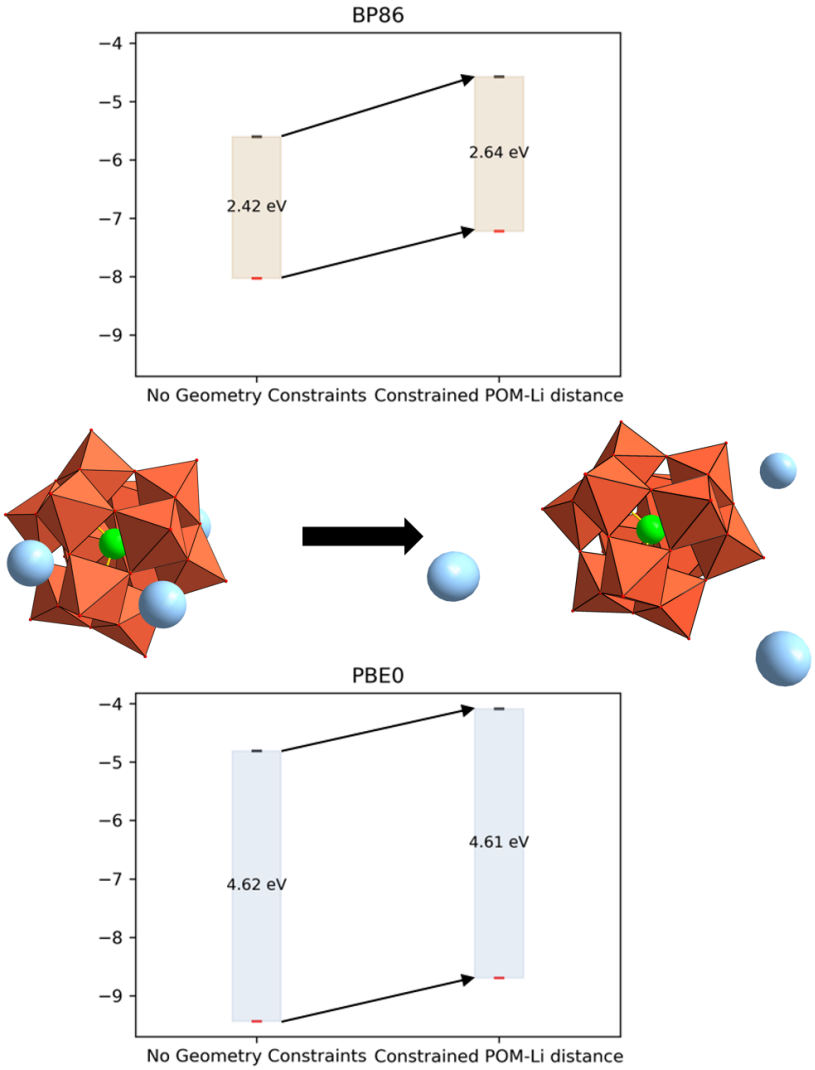

Figure 7. The changes in the frontier orbital energies of the Keggin α-$[PW_{12}O_{40}]^{3-}$ POM upon constraining the POM-cation distance to 9.1Å. The energy of the LUMO is indicated by black horizontal lines, the energy of the HOMO is indicated by red horizontal line and, the HOMO-LUMO gap (eV) is

labelled in between. The top plot shows data for BP86 functional calculations, the bottom plot shows data for BP86 functional calculations. Polyhedral and ball and ball-and-stick model representation of the α-$[W_{18}O_{54}(PO_4)_2]^{6-}$ POM, the left model shows an optimized geometry with no geometry constraint, the right model show an optimized geometry where the POM-Li^+ distance was constrained (cation-heteroatom distance = 9.1 Å). Colour code: heteropoly anions: light red polyhedra; P: green; O: red; Li: pale blue.

In addressing these challenges, this work incorporates a more refined approach by constraining Li^+ cations' geometry to replicate solvent-mediated distances accurately. This adjustment is pivotal in transitioning from a simplified COSMO simulation to a representation that respects the empirical data, thereby providing a more authentic depiction of POM-cation interactions within a solvent. Moreover, the discussion extends to evaluating the COSMO model's efficacy as a proxy for explicit counter-cation modelling in solution. This understanding underscores the broader implications of our findings, driving future research directions and potential applications in molecular electronics and POM-based devices.

Notably, this change in frontier orbital energy meant that models which included solvent effects gave frontier orbital energies which were largely independent of counter-cation, that is, the frontier orbital energy was not dependent on the identity of the counter-cation or even whether they were present at all. We found that the counter-cations, when compared to the water solvated naked POM, had minimal additional effects on frontier orbital energies in terms of stabilisation. These results indicate that solid-state POMs can be accurately modelled using the continuum solvent model alone; this is significant because it is more computationally efficient approach. The implication of this finding is that models which include aqueous solvent (common given the common aqueous synthesis of POMs) need not include explicit counter-cations. These same patterns as detailed for the Keggin α-$[PW_{12}O_{40}]^{3-}$ POM are replicated in the other POMs modelled – the results of these calculations are given in the supplementary information. This is significant for future work since it means computationally less expensive calculations without a meaningful reduction in accuracy.

Conclusion

This investigation into the explicit modelling of POM counter-cations, both in solid state and in solution, has yielded insights that are crucial for the integration of POMs into molecular electronics, particularly as components of single-molecule electronic devices. That theoretical models should include explicit counter-cations when calculating frontier orbital energies in the solid state, but it is more computationally efficient to forgo them in solution. Our study, by employing a combination of Density Functional Theory (DFT) calculations and the Conductor-like Screening Model (COSMO), has addressed key challenges in accurately representing the environmental effects on POMs, especially the influence of counter-cations and solvent molecules. The explicit inclusion of counter-cations remains imperative for accurately simulating the conditions relevant to POM-based electronic devices.

Another significant finding of our work is the identification and correction of the overestimation of counter-cation proximity to POM anions by the COSMO model. This overestimation, which leads to an overstabilization of frontier orbital energies, was effectively mitigated by constraining the geometry of Li+ cations, thus providing a more realistic depiction of POM-cation interactions in solvent environments. This methodological enhancement underscores the importance of considering physical solvent effects and counter-cation distances in theoretical models to ensure accuracy and relevance to real-world applications. Furthermore, the differential impact of various exchange-correlation functionals on the frontier orbital energies and HOMO-LUMO gaps of POMs underscores the necessity of further work which is grounded in empirical work. Given the magnitude of the discrepancy between these methods, it should be established which is gives the more realistic results.

In conclusion, our work not only advances the theoretical modelling of POMs but also contributes to the broader quest for novel materials capable of powering the next generation of molecular electronics. By bridging gaps in our understanding of POM-cation interactions and the role of the solvent environment, this study lays a solid foundation for future endeavours in the design and development of POM-based electronic components.

ASSOCIATED CONTENT

Data Availability. The datasets generated using DFT calculations are available in the ioChem-BD database (ioChem-Find: Home (iochem-bd.org)). https://doi.org/10.19061/iochem-bd-6-298

Supporting Information. The supporting information detailing computational information is available, see SI document.

AUTHOR INFORMATION

Corresponding Author

Corresponding Authors *Correspondence and requests for materials should be addressed to Vihar P. Gerorgiev (Vihar.Georgiev@glasgow.ac.uk) and Laia Vilà-Nadal (laia.vila−nadal@chem.gla.ac.uk)

Author Contributions

L.V.-N. conceived the idea, designed the project and together with M.J.A. and J.J. designed the modelling strategy. M.J.A. and J.J. did all the theoretical calculations. J.J. analysed the data together with L.V.-N. and V.P.G. J.J. wrote the paper and prepared the graphics with input from V.P.G. and L.V.-N. L. V. -N. and V. P.G. raised the funding and supervised the research.

ACKNOWLEDGMENTS & FUNDING SOURCES

Work financed by the University of Glasgow and the Engineering and Physical Sciences Research Council Grants (EP/S030603/1; EP/V048341/1; EP/S031170/1), Royal Society of Chemistry RSC-Hardship Grant (COVID-19). We also thank the University of Glasgow (UofGla) Early Career Development Programme (ECDP) 2021, the UofGla Reinvigorating Research Scheme 2022, and the School of Chemistry for long-lasting support. Theoretical results obtained using the ARCHIE-WeSt High-Performance Computer (www.archie-west.ac.uk) based at the University of Strathclyde.

References

1. Pope, M. T. Polyoxo Anions: Synthesis and Structure; Elsevier Inc., **2013**. DOI: https://doi.org/10.1016/b978-0-12-409547-2.01043-x.

2. Misra, A.; Kozma, K.; Streb, C.; Nyman, M. Beyond Charge Balance: Counter-Cations in Polyoxometalate Chemistry. *Angewandte Chemie - International Edition* **2020**, 59 (2), 596–612. DOI: https://doi.org/10.1002/anie.201905600.

3. Ammam, M. Polyoxometalates: Formation, Structures, Principal Properties, Main Deposition Methods and Application in Sensing. *J. Mater. Chem. A Mater* **2013**, 1 (21), 6291–6312. DOI: https://doi.org/10.1039/C3TA01663C.

4. Pope, M. T. Heteropoly and Isopoly Oxometalates, 1st ed.; Springer-Verlag Berlin Heidelberg: Berlin, **1983**.

5. Pope, M.T. (2011). Polyoxometalates. In Encyclopedia of Inorganic and Bioinorganic Chemistry, R.A. Scott (Ed.). https://doi.org/10.1002/9781119951438.eibc0185

6. Long, D. L.; Tsunashima, R.; Cronin, L. Polyoxometalates: Building Blocks for Functional Nanoscale Systems. *Angewandte Chemie International Edition* **2010**, 49 (10), 1736–1758. DOI: https://doi.org/10.1002/ANIE.200902483.

7. Hill, C. L. Progress and Challenges in Polyoxometalate-Based Catalysis and Catalytic Materials Chemistry. *J. Mol. Catal. A Chem.* **2007**, 262 (1), 2–6. DOI: https://doi.org/https://doi.org/10.1016/j.molcata.2006.08.042.

8. Samaniyan, M.; Mirzaei, M.; Khajavian, R.; Eshtiagh-Hosseini, H.; Streb, C. Heterogeneous Catalysis by Polyoxometalates in Metal–Organic Frameworks. *ACS Catal.* **2019**, 9 (11), 10174–10191. DOI: https://doi.org/10.1021/acscatal.9b03439.

9. Ju, F.; Vandervelde, D.; Nikolla, E. Molybdenum-Based Polyoxometalates as Highly Active and Selective Catalysts for the Epimerization of Aldoses. *ACS Catal.* **2014**, 4 (5), 1358–1364. DOI: https://doi.org/10.1021/cs401253z.

10. Rhule, J. T.; Hill, C. L.; Judd, D. A.; Schinazi, R. F. Polyoxometalates in Medicine. *Chem Rev* **1998**, 98 (1), 327–358. DOI: https://doi.org/10.1021/cr960396q

11. Čolović MB, Lacković M, Lalatović J, Mougharbel AS, Kortz U, Krstić DZ. Polyoxometalates in Biomedicine: Update and Overview. Curr Med Chem. 2020;27(3):362-379. DOI: https://doi.org/10.2174/0929867326666190827153532

12. Lentink, S.; Salazar Marcano, D. E.; Moussawi, M. A.; Parac-Vogt, T. N. Exploiting Interactions between Polyoxometalates and Proteins for Applications in (Bio)Chemistry and Medicine. *Angew. Chem. Int. Ed. 2023, 62, e202303817.* DOI: https://doi.org/10.1002/anie.202303817.

13. Zhang, Y.; Li, Y.; Guo, H.; Guo, Y.; Song, R. Recent Advances in Polyoxometalate-Based Materials and Their Derivatives for Electrocatalysis and Energy Storage. *Mater Chem Front* **2023**. DOI: https://doi.org/10.1039/d3qm01000g.

14. Pakulski, D.; Gorczyński, A.; Brykczyńska, D.; Montes-García, V.; Czepa, W.; Janica, I.; Bielejewski, M.; Kubicki, M.; Patroniak, V.; Samorì, P.; Ciesielski, A. New Anderson-Based Polyoxometalate Covalent Organic Frameworks as Electrodes for Energy Storage Boosted Through Keto-Enol Tautomerization. *Angewandte Chemie International Edition* **2023**, 62 (32), e202305239. DOI: https://doi.org/https://doi.org/10.1002/anie.202305239.

15. Anjass, M.; Lowe, G. A.; Streb, C. Molecular Vanadium Oxides for Energy Conversion and Energy Storage: Current Trends and Emerging Opportunities. *Angewandte Chemie - International Edition* **2021**, 60 (14), 7522–7532. DOI: https://doi.org/10.1002/anie.202010577.

16. Kondinski, A.; Ghorbani-Asl, M. Polyoxoplatinates as Covalently Dynamic Electron Sponges and Molecular Electronics Materials. *Nanoscale Adv.* **2021**, 3 (19), 5663–5675. DOI: https://doi.org/10.1039/D1NA00387A.

17. Naher, M.; Roemer, M.; Koutsantonis, G. A.; Low, P. J. Metal Complexes for Molecular Electronics, Third Edit.; Elsevier, **2021**; Vol. 9. DOI: https://doi.org/10.1016/b978-0-12-409547-2.14952-2.

18. Chen, X.; Zhou, Y.; Roy, V. A. L.; Han, S. T. Evolutionary Metal Oxide Clusters for Novel Applications: Toward High-Density Data Storage in Nonvolatile Memories. *Adv. Mater. 2018, 30, 1703950*. DOI: https://doi.org/10.1002/ADMA.201703950.

19. Moors, M.; Monakhov, K. Y. Capacitor or Memristor: Janus Behavior of Polyoxometalates. ACS Appl Electron Mater 2023. DOI: https://doi.org/10.1021/acsaelm.3c01751

20. Gao, Y.; Choudhari, M.; Such, G. K.; Ritchie, C. Polyoxometalates as Chemically and Structurally Versatile Components in Self-Assembled Materials. *Chem. Sci.* **2022**, 13 (9), 2510–2527. DOI: https://doi.org/10.1039/d1sc05879g.

21. Busche, C.; Vilà-Nadal, L.; Yan, J.; Miras, H. N.; Long, D. L.; Georgiev, V. P.; Asenov, A.; Pedersen, R. H.; Gadegaard, N.; Mirza, M. M.; Paul, D. J.; Poblet, J. M.; Cronin, L. Design and Fabrication of Memory Devices Based on Nanoscale Polyoxometalate Clusters. *Nature* **2014**, 515 (7528), 545–549. DOI: https://doi.org/10.1038/nature13951.

22. Chen, X.; Huang, P.; Zhu, X.; Zhuang, S.; Zhu, H.; Fu, J.; Nissimagoudar, A. S.; Li, W.; Zhang, X.; Zhou, L.; Wang, Y.; Lv, Z.; Zhou, Y.; Han, S.-T. Keggin-Type Polyoxometalate Cluster as an Active Component for Redox-Based Nonvolatile Memory. Nanoscale Horiz **2019**, 4 (3), 697–704. DOI: https://doi.org/10.1039/C8NH00366A.

23. López, X.; Fernández, J. A.; Poblet, J. M. Redox Properties of Polyoxometalates: New Insights on the Anion Charge Effect. Journal of the Chemical Society. *Dalton Transactions* **2006**, 6 (9), 1162–1167. DOI: https://doi.org/10.1039/b507599h.

24. Ritchie, C.; Streb, C.; Thiel, J.; Mitchell, S. G.; Miras, H. N.; Long, D. L.; Boyd, T.; Peacock, R. D.; McGlone, T.; Cronin, L. Reversible Redox Reactions in an Extended Polyoxometalate Framework Solid. *Angewandte Chemie - International Edition* **2008**, 47 (36), 6881–6884. DOI: https://doi.org/10.1002/anie.200802594.

25. Monakhov, K. Y.; Moors, M.; Kögerler, P. Chapter Nine - Perspectives for Polyoxometalates in Single-Molecule Electronics and Spintronics. In Advances in Inorganic Chemistry; van Eldik, R.,

Cronin, L., Eds.; *Academic Press*, **2017**, 69, 251–286. DOI: https://doi.org/https://doi.org/10.1016/bs.adioch.2016.12.009.

26. Wu, C.; Qiao, X.; Robertson, C. M.; Higgins, S. J.; Cai, C.; Nichols, R. J.; Vezzoli, A. A Chemically Soldered Polyoxometalate Single-Molecule Transistor. *Angewandte Chemie* **2020**, 132 (29), 12127–12132. DOI: https://doi.org/10.1002/ange.202002174.

27. Jacobs, J.; Vilà-Nadal, L.; Georgiev, V. Atomistic Modeling of $[W_{18}O_{54}(SeO_3)_2]^{4-}$ Polyoxometalates (POM) Molecules in the Presence of Counter-Cations for Memory Device Applications. *Proceedings of the IEEE International Conference on Nanoelectronics*, Guijon, Spain, 8-11 July **2024**, Accepted/ page number pending.

28. Georgiev, V. P.; Amoroso, S. M.; Ali, T. M.; Vilà-Nadal, L.; Busche, C.; Cronin, L.; Asenov, A. Comparison Between Bulk and FDSOI POM Flash Cell: A Multiscale Simulation Study. *IEEE Trans Electron Devices* **2015**, 62 (2), 680–684. DOI: https://doi.org/10.1109/TED.2014.2378378.

29. Vilà-Nadal, L.; Mitchell, S. G.; Markov, S.; Busche, C.; Georgiev, V.; Asenov, A.; Cronin, L. Towards Polyoxometalate-Cluster-Based Nano-Electronics. *Chemistry - A European Journal* **2013**, 19 (49), 16502–16511. DOI: https://doi.org/10.1002/chem.201301631.

30. Badami, O.; Sadi, T.; Adamu-Lema, F.; Lapham, P.; Mu, D.; Georgiev, V.; Ding, J.; Asenov, A. A Kinetic Monte Carlo Study of Retention Time in a POM Molecule-Based Flash Memory. *IEEE Trans. Nanotechnol* **2020**, 19, 704–710. DOI: https://doi.org/10.1109/TNANO.2020.3016182.

31. N. S., S., Basu, N., Cahay, M., M. N., S., Mal, S.S. and Das, P.P. (2020), Redox-Active Vanadium-Based Polyoxometalate as an Active Element in Resistive Switching Based Nonvolatile Molecular Memory. Phys. Status Solidi A, 217: 2000306. DOI: https://doi.org/10.1002/pssa.202000306

32. Huez, C.; Renaudineau, S.; Volatron, F.; Proust, A.; Vuillaume, D. Experimental Observation of the Role of Countercations in Modulating the Electrical Conductance of Preyssler-Type Polyoxometalate Nanodevices. *Nanoscale* **2023**, 15 (25), 10634–10641. DOI: https://doi.org/10.1039/D3NR02035E.

33. López, X.; Carbó, J. J.; Bo, C.; Poblet, J. M. Structure, Properties and Reactivity of Polyoxometalates: A Theoretical Perspective. *Chem. Soc. Rev.* **2012**, 41 (22), 7537–7571. DOI: https://doi.org/10.1039/c2cs35168d.

34. Poblet, J. M.; López, X.; Bo, C. Ab Initio and DFT Modelling of Complex Materials: Towards the Understanding of Electronic and Magnetic Properties of Polyoxometalates. *Chem. Soc. Rev.* **2003**, 32 (5), 297–308. DOI: https://doi.org/10.1039/B109928K.

35. Steffler, F.; De Lima, G. F.; Duarte, H. A. The Effect of the Heteroatom (X=P, As, Si and Ge) on the Geometrical and Electronic Properties of α-Keggin Polyoxometalates (M=Mo, W and Nb) – A DFT Investigation. *J. Mol. Struct.* **2020**, 1213, 0–5. DOI: https://doi.org/10.1016/j.molstruc.2020.128159.

36. Ravelli, D.; Dondi, D.; Fagnoni, M.; Albini, A.; Bagno, A. Predicting the UV Spectrum of Polyoxometalates by TD-DFT. *J. Comput. Chem.* **2011**, 32 (14), 2983–2987. DOI: https://doi.org/https://doi.org/10.1002/jcc.21879.

37. Bo, C.; Poblet, J. M. Electronic Properties and Molecular Simulations of Polyoxometalates. Isr *J. Chem.* **2011**, 51 (2), 228–237. DOI: https://doi.org/10.1002/ijch.201100017.

38. Vilà-Nadal, L.; Romo, S.; López, X.; Poblet, J. M. Structural and Electronic Features of Wells-Dawson Polyoxometalates. *NATO Science for Peace and Security Series B: Physics and Biophysics* **2012**, 171–183. DOI: https://doi.org/10.1007/978-94-007-5548-2-10.

39. López, X.; Maestre, J. M.; Bo, C.; Poblet, J. M. Electronic Properties of Polyoxometalates: A DFT Study of α/β-$[XM_{12}O_{40}]^{n-}$ Relative Stability (M=W, Mo and X a Main Group Element). *J. Am. Chem. Soc* **2001**, 123 (39), 9571–9576. DOI: https://doi.org/10.1021/ja010768z.

40. López, X.; Fernández, J. A.; Romo, S.; Paul, J. F.; Kazansky, L.; Poblet, J. M. Are the Solvent Effects Critical in the Modeling of Polyoxoanions? *J. Comput. Chem.* **2004**, 25 (12), 1542–1549. DOI: https://doi.org/10.1002/jcc.20083.

41. Miró, P.; Poblet, J. M.; Ávalos, J. B.; Bo, C. Towards a Computational Treatment of Polyoxometalates in Solution Using QM Methods and Explicit Solvent Molecules. *Can. J. Chem.* **2009**, 87 (10), 1296–1301. DOI: https://doi.org/10.1139/V09-059.

42. Monakhov, K. Yu. Implication of Counter-Cations for Polyoxometalate-Based Nano-Electronics. *Comments on Inorganic Chemistry* **2022**, 44 (1), 1–10. DOI: https://doi.org/10.1080/02603594.2022.2157409.

43. Misra, A.; Kozma, K.; Streb, C.; Nyman, M. Beyond Charge Balance: Counter-Cations in Polyoxometalate Chemistry. *Angewandte Chemie International Edition* **2020**, 59 (2), 596–612. DOI: https://doi.org/https://doi.org/10.1002/anie.201905600.

44. Yorur Goreci, C. Synthesis and Comparative Spectroscopic Studies, HOMO–LUMO Analysis and Molecular Docking Studies of 3,3′-(1,4-Phenylene)Bis[2-(6-Chloropyridin-3-Yl)Prop 2-Enenitrile] Based on DFT. *J. Mol. Struct.* **2022**, 1263, 133149. DOI: https://doi.org/10.1016/J.MOLSTRUC.2022.133149.

45. Kissling, G. P.; Ruhstaller, B.; Pernstich, K. P. Measuring Frontier Orbital Energy Levels of OLED Materials Using Cyclic Voltammetry in Solution. *Org. Electron.* **2023,** 122, 106888. DOI: https://doi.org/10.1016/J.ORGEL.2023.106888.

46. Klamt, A. The COSMO and COSMO-RS Solvation Models. *Wiley Interdisciplinary Reviews: Computational Molecular Science*. Blackwell Publishing Inc. January 1, **2018**. DOI: https://doi.org/10.1002/wcms.1338.

47. Klamt, A.; Schüürmann, G. COSMO: A New Approach to Dielectric Screening in Solvents with Explicit Expressions for the Screening Energy and Its Gradient. *J. Chem. Soc., Perkin Trans.* 2 **1993**, 5, 799–805. DOI: https://doi.org/10.1039/P29930000799.

48. Pye, C. C.; Ziegler, T.; Van Lenthe, E.; Louwen, J. N. An Implementation of the Conductor-like Screening Model of Solvation within the Amsterdam Density Functional Package—Part II.

COSMO for Real Solvents. *Can. J. Chem.* **2009**, 87 (7), 790–797.DOI: https://doi.org/10.1139/V09-008

49. Tomasi, J.; Mennucci, B.; Cammi, R. Quantum Mechanical Continuum Solvation Models. *Chem. Rev*. **2005**, 105 (8), 2999–3093. DOI: https://doi.org/10.1021/cr9904009.

50. Perdew, J. P.; Ernzerhof, M.; Burke, K.; Rationale for mixing exact exchange with density functional approximations. J. Chem. Phys. 8 December 1996; 105 (22): 9982–9985. https://doi.org/10.1063/1.472933

51. Ernzerhof, M.; Scuseria, G. E. Assessment of the Perdew–Burke–Ernzerhof exchange-correlation functional. J. Chem. Phys. 15 March 1999; 110 (11): 5029–5036. https://doi.org/10.1063/1.478401

52. Adamo, C.; Barone, V. Carlo Adamo, Vincenzo Barone; Toward reliable density functional methods without adjustable parameters: The PBE0 model. J. Chem. Phys. 1 April 1999; 110 (13): 6158–6170. https://doi.org/10.1063/1.478522

53. Becke, A. D. (1988). Density-functional exchange-energy approximation with correct asymptotic behavior. *Physical Review A*, *38*(6), 3098–3100. https://doi.org/10.1103/PhysRevA.38.3098

54. Perdew, J. P. (1986). BP86 b). Phys. Rev. B, 33, 8822–8824.

55. Pye, C. C.; Ziegler, T. An Implementation of the Conductor-like Screening Model of Solvation within the Amsterdam Density Functional Package. *Theor. Chem. Acc.* **1999**, 101 (6), 396–408. DOI: https://doi.org/10.1007/s002140050457.

56. te Velde, G.; Bickelhaupt, F. M.; Baerends, E. J.; Fonseca Guerra, C.; van Gisbergen, S. J. A.; Snijders, J. G.; Ziegler, T. Chemistry with ADF. *J. Comput. Chem.* **2001**, 22 (9), 931–967. DOI: https://doi.org/https://doi.org/10.1002/jcc.1056.

57. Becke, A. D. Density-Functional Exchange-Energy Approximation with Correct Asymptotic Behavior. *Phys. Rev. A.* **1988**, 38 (6), 3098–3100. DOI: https://doi.org/10.1103/PhysRevA.38.3098.

58. Perdew, J. P. Density-Functional Approximation for the Correlation Energy of the Inhomogeneous Electron Gas. *Phys. Rev. B.* **1986**, 33 (12), 8822–8824. DOI: https://doi.org/10.1103/PhysRevB.33.8822.

59. Ernzerhof, M.; Scuseria, G. E. Assessment of the Perdew–Burke–Ernzerhof Exchange-Correlation Functional. *J. Chem. Phys.* **1999**, 110 (11), 5029–5036. DOI: https://doi.org/10.1063/1.478401.

60. Stephens, P. J.; Devlin, F. J.; Chabalowski, C. F.; Frisch, M. J. Ab Initio Calculation of Vibrational Absorption and Circular Dichroism Spectra Using Density Functional Force Fields. *J. Phys. Chem.* **1994**, 98 (45), 11623–11627. DOI: https://doi.org/10.1021/j100096a001.

61. Grimme, S. Accurate Description of van Der Waals Complexes by Density Functional Theory Including Empirical Corrections. *J. Comput. Chem.* **2004**, 25 (12), 1463–1473. DOI: https://doi.org/https://doi.org/10.1002/jcc.20078.

62. Van Lenthe, E.; Baerends, E. J. Optimized Slater-Type Basis Sets for the Elements 1–118. *J. Comput. Chem.* **2003**, 24 (9), 1142–1156. DOI: https://doi.org/https://doi.org/10.1002/jcc.10255.

63. Lapham, P.; Vilà-Nadal, L.; Cronin, L.; Georgiev, V. P. Influence of the Contact Geometry and Counterions on the Current Flow and Charge Transfer in Polyoxometalate Molecular Junctions: A Density Functional Theory Study. *The Journal of Physical Chemistry C.* **2021**, 125 (6), 3599–3610. DOI: https://doi.org/10.1021/acs.jpcc.0c11038.

64. Ravelli, D.; Dondi, D.; Fagnoni, M.; Albini, A.; Bagno, A. Predicting the UV Spectrum of Polyoxometalates by TD-DFT. *J. Comput. Chem.* **2011**, 32 (14), 2983–2987. DOI: https://doi.org/https://doi.org/10.1002/jcc.21879.

65. van Lenthe, E.; Baerends, E. J.; Snijders, J. G. Relativistic Total Energy Using Regular Approximations. J Chem Phys 1994, 101 (11), 9783–9792. DOI: https://doi.org/10.1063/1.467943.

66. van Lenthe, E.; Leeuwen, R. van; Baerends, E. J.; Snijders, J. G. Relativistic Regular Two-Component Hamiltonians. *Int. J. Quantum. Chem.* **1996**, 57 (3), 281–293. DOI: https://doi.org/10.1002/(SICI)1097-461X(1996)57:3<281::AID-QUA2>3.0.CO;2-U

67. van Lenthe, E.; Ehlers, A.; Baerends, E.-J. Geometry Optimizations in the Zero Order Regular Approximation for Relativistic Effects. *J. Chem. Phys.* **1999**, 110 (18), 8943–8953. DOI: https://doi.org/10.1063/1.478813.

68. van Lenthe, E.; Snijders, J. G.; Baerends, E. J. The Zero-Order Regular Approximation for Relativistic Effects: The Effect of Spin–Orbit Coupling in Closed Shell Molecules. J Chem Phys 1996, 105 (15), 6505–6516. DOI: https://doi.org/10.1063/1.472460.

69. van Lenthe, E., van Leeuwen, R., Baerends, E.J. and Snijders, J.G. (1996), Relativistic regular two-component Hamiltonians. Int. J. Quantum Chem., 57: 281-293. DOI: https://doi.org/10.1002/(SICI)1097-461X(1996)57:3<281::AID-QUA2>3.0.CO;2-U

70. Klamt, A. COSMO-RS: From Quantum Chemistry to Fluid Phase Thermodynamics and Drug Design; Elsevier, 2005. DOI: https://doi.org/10.1016/B978-0-444-64235-6.50003-6

71. Allinger, N. L.; Zhou, X.; Bergsma, J. Molecular Mechanics Parameters. Journal of Molecular Structure: THEOCHEM 1994, 312 (1), 69–83. DOI: https://doi.org/10.1016/S0166-1280(09)80008-0

72. Alvarez, S. A Cartography of the van Der Waals Territories. *Dalton Transactions* **2013**, 42 (24), 8617–8636. DOI: https://doi.org/10.1039/C3DT50599E.

73. Vilà-Nadal, L.; Cronin, L. Design and Synthesis of Polyoxometalate-Framework Materials from Cluster Precursors. *Nat. Rev. Mater.* **2017**, 2 (10), 17054. DOI: https://doi.org/10.1038/natrevmats.2017.54.

74. Bridgeman, A. J.; Cavigliasso, G. Structure and Bonding in $[M_6O_{19}]^{n-}$ Isopolyanions. *Inorg Chem* **2002**, 41 (7), 1761–1770. DOI: https://doi.org/10.1021/ic011086f.

75. Malcolm, D.; Vilà-Nadal, L. Computational Study into the Effects of Countercations on the $[P_8W_{48}O_{184}]^{40-}$ Polyoxometalate Wheel. *ACS Organic & Inorganic Au* **2023**. 3, 5, 274–282 DOI: https://doi.org/10.1021/acsorginorgau.3c00014.

76. Kaledin, A. L.; Yin, Q.; Hill, C. L.; Lian, T.; Musaev, D. G. Ion-Pairing in Polyoxometalate Chemistry: Impact of Fully Hydrated Alkali Metal Cations on Properties of the Keggin $[PW_{12}O_{40}]^{3-}$ Anion. *Dalton Transactions* **2020**, 49 (32), 11170–11178. DOI: https://doi.org/10.1039/D0DT02239J.

77. Thompson, J. A.; Vilà-Nadal, L. Computation of ^{31}P NMR Chemical Shifts in Keggin−based Lacunary Polyoxotungstates. *Dalton Transactions* **2024**, 53 (2), 564–571. DOI: https://doi.org/10.1039/D3DT02694A.